

Band geometry induced electro-optic effect and polarization rotation

M. Maneesh Kumar,^{1,*} Sanjay Sarkar,^{1,*} and Amit Agarwal^{1,†}

¹*Department of Physics, Indian Institute of Technology Kanpur, Kanpur 208016*

Electric field-induced modulation of the optical properties is crucial for amplitude and phase modulators used in photonic devices. Here, we present a comprehensive study of the band geometry-induced electro-optic effect, specifically focusing on the Fermi surface and disorder-induced contributions. These contributions are crucial for metallic and semimetallic systems and for optical frequencies comparable to or smaller than the scattering rates. We highlight the importance of the quantum metric and metric connection in generating the electro-optic effect in parity-time reversal (\mathcal{PT}) symmetric systems such as CuMnAs. Our findings establish the electro-optic effect as a novel tool to probe band geometric effects and open new avenues to design electrically controlled efficient amplitude and phase modulators for photonic applications.

I. Introduction

Electro-optical effects showcase the remarkable ability of quantum materials to transform their optical properties under the influence of an applied dc electric field. Specifically, for linear electro-optical (EO) or Pockels effect [1–5], the change in the refractive index (RI) is proportional to the strength of the applied dc electric field. This phenomenon underpins the functionality of EO materials as amplitude and phase modulators, which enable electrical tunability and manipulation of the optical parameters such as amplitude, phase, and polarization [6–8], for a variety of applications in photonic devices. There is immense interest in the exciting phenomena of EO effects and polarization rotation in optical experiments [9–12]. Earlier studies have focused on material systems such as organic materials [13, 14], liquid crystals [15], chiral topological semimetals [16–18], zinc blends [19], certain trigonal and piezoelectric crystals [20, 21], Ferroelectric oxide materials [22], Si₃N₄ platforms [23], silicone waveguides [24], and on certain stoichiometric samples [25–28]. The EO modulators based on epitaxial BaTiO₃ integrated on silicon [29] play a pivotal role in optical communication.

Despite extensive material-based studies of EO effects, a comprehensive theoretical exploration of the phenomena of EO effect induced by nonlinear optical susceptibilities is still lacking. Specifically, the contributions to the nonlinear optical susceptibilities induced by Fermi surface effects and scattering with impurities have not been explored earlier. These contributions are essential for metallic and semimetallic systems and for exploring low-frequency EO regimes. Recently, this effect has been studied in chiral topological semimetals [30], revealing that the second-order response includes contributions from the shift current, injection current, and nonlinear anomalous current induced by the Berry curvature. Here, we develop a generalized theory of the linear EO effect, which works for all systems without any symmetry con-

straints. Using the density-matrix based quantum kinetic theory framework, we calculate the second-order optical response at finite optical frequencies. We retain all Fermi surface and Fermi sea contributions and disorder effects to identify six unique contributions to the linear EO effect. We denote these contributions as shift, injection, Drude, anomalous, higher-order pole, and double resonant contributions [31]. As an example to demonstrate our work, we focus on an antiferromagnetic material CuMnAs, which breaks parity (\mathcal{P}) and time-reversal symmetry (\mathcal{T}) but is \mathcal{PT} symmetric. In a \mathcal{PT} symmetric system, the Berry curvature and the symplectic connection—the imaginary parts of the quantum geometric tensor (QGT), and the quantum geometric connection (QGC) vanish. We show that the dominant contribution in the linear EO effect in \mathcal{PT} symmetric systems emerges from the quantum metric and the metric connection, the real parts of QGT and QGC, respectively. More interestingly, we show that the dominant EO effect arises for optical energies lesser than the chemical potential. This highlights that the Fermi surface effects play a significant role in EO effects.

Our paper is structured as follows: In Sec. II, we develop the framework for understanding the EO effect starting from Maxwell’s equations. In Sec. III, we explore the linear EO effect, focusing on the relationship between birefringence and the applied static electric field. In Sec. IV, we introduce the distinct band geometric contributions to optical susceptibilities, capturing the Fermi sea, Fermi surface, and disorder effects. We demonstrate our results in Sec. V, for a model system of CuMnAs, a \mathcal{PT} -symmetric material, with broken \mathcal{P} and \mathcal{T} -symmetry. Finally, in Sec. VI, we summarise our work.

II. The electro-optic effect

In this section, we employ Maxwell’s equations to calculate the modulation of frequency-dependent refractive indices in a medium subjected to a dc electric field. The spatio-temporal evolution of the electric field propagat-

* M.M.K. and S.S. contributed equally to this manuscript.

† amitag@iitk.ac.in

ing in a medium is given by [32, 33],

$$\nabla^2 \mathbf{E}(\mathbf{r}, t) = \frac{\partial}{\partial t} \left[\mu \mathbf{j}_f + \epsilon \mu \frac{\partial \mathbf{E}(\mathbf{r}, t)}{\partial t} \right]. \quad (1)$$

Here, ϵ (μ) is the static permittivity (permeability) of the medium, and \mathbf{j}_f is the free charge current density. We consider a light beam propagating with wave vector \mathbf{q} along the z -axis (\hat{z}) with its polarization confined to the x - y plane. An external bias voltage (static or slowly varying) is applied along the y -axis, resulting in a dc electric field $\mathbf{E}^d = E_y^d \hat{y}$. Thus, for a monochromatic light of frequency ω , the dominant electron current oscillating with a frequency ω and linear in the optical field strength $E(\omega)$, is given by [2, 34],

$$j_a(\omega) = \sigma_{ab}(\omega) E_b(\omega) + \sigma_{abc}^{(2)}(\omega; \omega, 0) E_b(\omega) E_c^d(0). \quad (2)$$

Here, the first term denotes the linear conductivity, and the second term represents the NL current contribution responsible for the linear electro-optic effect. In Eq. (2), the summation over repeated indices is implied. We will focus on the propagating plane wave solutions of Eq. (1), which have the form $\mathbf{E}(\omega) = \mathbf{E}_0 e^{i(\mathbf{q} \cdot \mathbf{r} - \omega t)}$. Using $\mathbf{E}(\omega)$, and Eq. (2) in Eq. (1), we obtain,

$$q^2 E_a = \frac{\omega^2}{c^2} \left[\frac{i \sigma_{ab} E_b}{\omega \epsilon_0} + \frac{i \sigma_{abc}^{(2)} E_b E_c}{\omega \epsilon_0} + E_a \right]. \quad (3)$$

$$(\tilde{N}^2 - N^2)^2 - (\tilde{N}^2 - N^2)[\eta^2 N^2 + (\chi_{yyy}^{(2)} + \chi_{xxy}^{(2)}) E_y^d] + \chi_{xxy}^{(2)} E_y^d (\eta^2 N^2 + \chi_{yyy} E_y^d) - (\chi_{xy} + \chi_{xyy}^{(2)} E_y^d)(\chi_{yx} + \chi_{yyx}^{(2)} E_y^d) = 0. \quad (7)$$

Solving the equation for roots of $(\tilde{N}^2 - N^2)$, we obtain the complex RI \tilde{N} to be

$$\tilde{N}_{\pm} = \sqrt{N^2 + \Theta_{\pm}}, \text{ where } \Theta_{\pm} \equiv \frac{1}{2} [\zeta \pm \sqrt{\zeta^2 - 4\xi}], \quad (8)$$

is a dc electric field and frequency-dependent function. Here, we have defined,

$$\zeta = [\eta^2 N^2 + (\chi_{yyy}^{(2)} + \chi_{xxy}^{(2)}) E_y^d], \quad (9)$$

and,

$$\begin{aligned} \xi = & \chi_{xxy}^{(2)} E_y^d (\eta^2 N^2 + \chi_{yyy}^{(2)} E_y^d) \\ & - (\chi_{xy} + \chi_{xyy}^{(2)} E_y^d)(\chi_{yx} + \chi_{yyx}^{(2)} E_y^d). \end{aligned} \quad (10)$$

Note that for $E_y^d \rightarrow 0$, we have $\zeta \rightarrow \eta^2 N^2$, and $\xi \rightarrow |\chi_{xy}|^2$. The complex RI can be tuned and controlled by varying E_y^d . \tilde{N}_{\pm} corresponds to two solutions for the effective propagating wavevectors, $\mathbf{q}_{\pm} = (\omega \tilde{N}_{\pm} / c) \hat{q}_{\pm}$, of the optical field. The complex RI can be expressed in terms of the refractivities (n_{\pm}) and the extinction (or absorption) coefficients (κ_{\pm}), $N_{\pm} = n_{\pm} + i\kappa_{\pm}$ [36].

Here, we have used $E_{a(b)} = E_{a(b)}(\omega)$ for brevity. Defining the finite frequency dielectric tensor [35], $\epsilon_{aa}(\omega) = 1 + \frac{i}{\omega \epsilon_0} \sigma_{aa}(\omega)$, we can express the above equation as,

$$\left[\left(\frac{cq}{\omega} \right)^2 - \epsilon_{aa}(\omega) \right] E_a = \frac{i}{\omega \epsilon_0} [\sigma_{ab} E_b (1 - \delta_{ab}) + \sigma_{abc}^{(2)} E_b E_c]. \quad (4)$$

We define the complex RI, $\tilde{N} = (cq/\omega)$ and $N_{aa}^2 = \epsilon_{aa}(\omega)$. The corresponding frequency-dependent susceptibility tensors are given by $\chi_{abc}^{(2)}(\omega; \omega, 0) = \frac{i}{\omega \epsilon_0} \sigma_{abc}^{(2)}(\omega; \omega, 0)$ and $\chi_{ab}(\omega) = \frac{i}{\omega \epsilon_0} \sigma_{ab}(\omega)$. Expressing Eq. (4) in terms of these, we obtain,

$$(\tilde{N}^2 - N_{aa}^2) E_a = \chi_{ab}(\omega) E_b (1 - \delta_{ab}) + \chi_{abc}^{(2)}(\omega; \omega, 0) E_b E_c. \quad (5)$$

Explicitly writing Eq. (5) for E_x and E_y in a matrix form, we have,

$$\begin{pmatrix} \tilde{N}^2 - N_{xx}^2 - \chi_{xxy}^{(2)} E_y^d & -\chi_{xy} - \chi_{xyy}^{(2)} E_y^d \\ -\chi_{yx} - \chi_{yyx}^{(2)} E_y^d & \tilde{N}^2 - N_{yy}^2 - \chi_{yyy}^{(2)} E_y^d \end{pmatrix} \begin{pmatrix} E_x \\ E_y \end{pmatrix} = 0. \quad (6)$$

For simplicity of notation and without loss of generality, we express $N_{xx} = N$ and $N_{yy} = N\sqrt{1 + \eta^2}$, where η is a parameterizing factor.

To have a non-trivial solution for E_x and E_y , the determinant of the matrix must vanish. This yields the following condition,

The eigenvectors corresponding to the propagating optical fields of Eq. (6) are given by,

$$\begin{pmatrix} E_x \\ E_y \end{pmatrix}_+ = |\mathbf{E}(\omega)| A_+ \begin{pmatrix} \chi_{xy} + \chi_{xyy}^{(2)} E_y^d \\ \Theta_+ - \chi_{xxy}^{(2)} E_y^d \end{pmatrix}, \quad (11)$$

and,

$$\begin{pmatrix} E_x \\ E_y \end{pmatrix}_- = |\mathbf{E}(\omega)| A_- \begin{pmatrix} \Theta_- - \chi_{yyy}^{(2)} E_y^d - \eta^2 N^2 \\ \chi_{yx} + \chi_{yyx}^{(2)} E_y^d \end{pmatrix}. \quad (12)$$

Here, $|\mathbf{E}(\omega)|$ is the strength of the incident field, and $A_{\pm} = A_{\pm}(\omega)$, are multiplicative factors normalizing the eigenvectors. These eigenvectors are tunable and can be electrically controlled by varying E_y^d .

An interesting consequence of the unequal refractive indices is the induced polarization rotation, $\Delta\phi$, for a linearly polarized light incident on the medium, and traverses through it. It can be quantified in terms of the finite birefringence given by $\Delta\tilde{n} = \text{Re}[\tilde{N}_+ - \tilde{N}_-]$. The linearly polarised light splits into two circularly polarised (CP) or elliptically polarised (EP) lights of opposite chirality upon entering the medium.

Consequently, upon exiting the medium, these superimpose into a linearly polarised light, with a rotated plane of polarisation w.r.t. the incident light. This frequency-dependent polarization rotation is given by [30, 37],

$$\Delta\tilde{\phi}(\omega) = \Delta\tilde{n}(\omega)\frac{\omega L}{c}. \quad (13)$$

Here, c is the speed of light in free space, and L is the length of the light path through the sample. This phenomenon is similar to the polarization rotation caused by the optical activity of chiral molecules [38]. However, in this case, the optical activity is controlled by a dc electric field.

In addition to the change in the refractive index, a static electric field can also induce a change in the absorption coefficient. This is instrumental for modulating the intensity of the propagating optical beams. Additionally, the two different absorption coefficients give rise to a frequency-dependent ellipticity of the propagating light and are also related to the dichroism. Analogous to the polarization rotation, the ellipticity ($\tan \varepsilon$) is given by [36],

$$\tan \varepsilon = -\tanh \left[\frac{\omega L}{2c} \Delta\tilde{\kappa} \right], \quad (14)$$

where we have defined $\Delta\tilde{\kappa} = (\tilde{\kappa}_+ - \tilde{\kappa}_-) = \text{Im}[\tilde{N}_+ - \tilde{N}_-]$.

In this section, we have developed a general theory on birefringence arising from the impact of a static dc

field captured via the nonlinear conductivity. In the next section, we focus on the linear EO effect.

III. Linear Electro-optic effect

The static electric-field dependent refractive indices obtained in Eq. (8), is a nonlinear function of E_y^d . Here, we focus on Pockels effect, which captures the linear E_y^d contribution to the polarization rotation. For this, we expand the altered complex RI in Eq. (8) in powers of E_y^d , to obtain

$$\zeta = \zeta^{(0)} + \zeta^{(1)} E_y^d. \quad (15)$$

Here, $\zeta^{(0)} = \eta^2 N^2$ and $\zeta^{(1)} = (\chi_{yyy} + \chi_{xxy})$. Similarly, we have,

$$\xi = \xi^{(0)} + \xi^{(1)} E_y^d + \xi^{(2)} (E_y^d)^2, \quad (16)$$

where $\xi^{(0)} = -\chi_{xy}\chi_{yx}$, $\xi^{(1)} = (\eta^2 N^2 \chi_{xxy} - \chi_{xy}\chi_{yxy} - \chi_{yx}\chi_{xyy})$, and $\xi^{(2)} = (\chi_{xxy}\chi_{yyy} + \chi_{xyy}\chi_{yxy})$. These expansions allow us to express \tilde{N}_\pm up to the first order of E_y^d as,

$$\tilde{N}_\pm = \frac{\sqrt{2N^2 + \zeta^{(0)} \pm \rho}}{\sqrt{2}} + \frac{\zeta^{(1)} (\rho \pm \zeta^{(0)}) \mp 2\xi^{(1)}}{2\sqrt{2}\rho\sqrt{2N^2 + \zeta^{(0)} \pm \rho}} E_y^d, \quad (17)$$

with, $\rho = \sqrt{[\zeta^{(0)}]^2 - 4\xi^{(0)}}$. The difference in complex RI arising from the Pockels effect is given by,

$$\Delta\tilde{N} = \tilde{N}_+ - \tilde{N}_- = \left[\frac{\zeta^{(1)} (\rho + \zeta^{(0)}) - 2\xi^{(1)}}{2\sqrt{2}\rho\sqrt{2N^2 + \zeta^{(0)} + \rho}} - \frac{\zeta^{(1)} (\rho - \zeta^{(0)}) + 2\xi^{(1)}}{2\sqrt{2}\rho\sqrt{2N^2 + \zeta^{(0)} - \rho}} \right] E_y^d. \quad (18)$$

The real and imaginary parts of the above expression capture the birefringence ($\Delta\tilde{n}$) and dichroism ($\Delta\tilde{\kappa}$) induced by the applied static electric field to first order. To evaluate these effects, we compute the second-order susceptibilities $\chi_{abc}^{(2)}(\omega; \omega, 0)$. The following section will detail this calculation using the density matrix-based quantum kinetic theory.

IV. second order Optical responses

In this section, we calculate the components of the second-order susceptibility $\chi_{abc}^{(2)}(\omega; \omega, 0)$ using the density-matrix based quantum kinetic theory formalism. We will include the impact of a finite Fermi surface and disorder in the second-order responses, which are usually neglected [30, 39]. We use the quantum Liouville equation (QLE) to calculate the non-equilibrium density matrix. The time evolution of the density matrix is given

by,

$$\frac{\partial \rho(\mathbf{k}, t)}{\partial t} + \frac{i}{\hbar} [\mathcal{H}, \rho(\mathbf{k}, t)] = 0. \quad (19)$$

Here, $\rho = \rho(\mathbf{k}, t)$ is the non-equilibrium density matrix, and $\mathcal{H} = \hat{H}_0 + \hat{H}_E$, with \hat{H}_0 describing the unperturbed Bloch Hamiltonian and \hat{H}_E is the perturbation Hamiltonian capturing the effect of the electric field. Using the dipole approximation in the length gauge [40, 41] framework, the light-matter interaction term can be expressed as,

$$\hat{H}_E = e\mathbf{E}(t) \cdot \hat{\mathbf{r}}. \quad (20)$$

Here, $\hat{\mathbf{r}}$ is the position operator, and $\mathbf{E}(t)$ is the time-dependent electric field. We perturbatively solve for the density matrix up to second order in the electric field strength. To solve Eq. (19), we use the adiabatic switching on of the perturbing fields, $\mathbf{E}(t) = \mathbf{E}e^{-i(\omega+i/\tau)t}$.

This approach, combined with the interaction picture, has been extensively used in literature for the perturbative solution of the density matrix [2, 42]. Incorporating such an adiabatic switching on approximation gives rise to a relaxation term in the kinetic equation. For the N th order density matrix ($\rho^{(N)} \propto E^N$), Eq. (19) yields [31, 43, 44],

$$\frac{\partial \rho^{(N)}}{\partial t} + \frac{i}{\hbar} [\hat{H}_0, \rho^{(N)}] + \frac{\rho^{(N)}}{\tau/N} = \frac{-ie\mathbf{E}}{\hbar} \cdot [\hat{\mathbf{r}}, \rho^{(N-1)}]. \quad (21)$$

In the above expression, we consider the relaxation time τ to be a constant. It accounts for the scattering of electrons with static and dynamic (phonons) impurities. We use this equation to obtain the density matrix of various orders in the electric field, as shown in Appendix A. Equipped with the expressions of the density matrices, we calculate the NL electric current using the expression,

$$\mathbf{j} = -e\text{Tr}[\rho\hat{\mathbf{v}}]. \quad (22)$$

Here, the velocity operator matrix, expressed in the eigenbasis of \hat{H}_0 , is given by $v_{pm}^a = v_m^a \delta_{pm} + (1 - \delta_{pm})i\omega_{pm}\mathcal{R}_{pm}^a\mathcal{R}_{pm}^a$, where $\mathcal{R}_{pm}^a = \langle u_{\mathbf{k},p} | \partial_{k_a} u_{\mathbf{k},m} \rangle$ with $|u_{\mathbf{k},m}\rangle$ being the m th band Bloch electron's wavefunction, is the interband Berry connection. From the current density, the second-order conductivities can be extracted via the relation,

$$j_a^{(2)}(\omega) = \sigma_{abc}^{(2)}(\omega; \omega, 0) E_b(\omega) E_c. \quad (23)$$

We obtain the second-order susceptibility from the second-order conductivity using the relation,

$$\chi_{abc}^{(2)}(\omega; \omega, 0) = \frac{i}{\omega\epsilon_0} \sigma_{abc}^{(2)}(\omega; \omega, 0). \quad (24)$$

Following Ref. [31], we express the second-order susceptibility into six distinct forms based on their origin. We denote these contributions as the shift (χ_{abc}^{Sh}), injection (χ_{abc}^{Inj}), Drude (χ_{abc}^{D}), anomalous (χ_{abc}^{An}), higher-order pole (χ_{abc}^{HOP}), and double resonant (χ_{abc}^{DR}) susceptibility, respectively. The shift and the injection currents arise from electron position and electron velocity transition (along current direction) during an optical interband excitation [45, 46]. These are both Fermi sea effects. The NL Drude contribution arises from the intraband transition and is a Fermi surface contribution [47]. The anomalous and the double resonant currents originate from the Fermi surface effects. The higher-order pole contribution occurs due to the velocity injection along the applied field direction, and it is a Fermi sea phenomenon. The NL susceptibilities in Eq. (8) is an aggregate of all these contributions. In addition to the contributions from the shift and injection currents [17], we highlight additional contributions to the NL conductivity [31]. The pairwise field-symmetrized NL susceptibilities are given by,

$$\chi_{abc}^{\text{Sh}} = -\frac{ie^3}{2\omega\epsilon_0\hbar^2} \sum_{m,p} \int_{\text{BZ}} [d\mathbf{k}] \omega_{mp} \tilde{g}_{mp}^\omega \left[g_{mp}^\omega \left(\Gamma_{mp}^{abc} - i\tilde{\Gamma}_{mp}^{abc} \right) + g_{mp}^0 \left(\Gamma_{mp}^{acb} - i\tilde{\Gamma}_{mp}^{acb} \right) \right] F_{mp}, \quad (25a)$$

$$\chi_{abc}^{\text{Inj}} = \frac{ie^3}{2\epsilon_0\omega\hbar^2} \sum_{m,p} \int_{\text{BZ}} [d\mathbf{k}] \partial_a(\omega_{mp}) g_0^\omega \left[g_{mp}^\omega \left(\mathcal{G}_{mp}^{bc} - i\frac{\Omega_{mp}^{bc}}{2} \right) + g_{mp}^0 \left(\mathcal{G}_{mp}^{cb} - i\frac{\Omega_{mp}^{cb}}{2} \right) \right] F_{mp}, \quad (25b)$$

$$\chi_{abc}^{\text{D}} = -\frac{ie^3}{2\epsilon_0\omega\hbar^2} \sum_m \int_{\text{BZ}} [d\mathbf{k}] \left[\frac{1}{\hbar} \partial_a \epsilon_{\mathbf{k},m} (\tilde{g}_0^\omega g_0^\omega + \tilde{g}_0^0 g_0^\omega) \partial_b \partial_c f_m \right], \quad (25c)$$

$$\chi_{abc}^{\text{An}} = -\frac{ie^3}{2\epsilon_0\omega\hbar^2} \sum_{m,p} \int_{\text{BZ}} [d\mathbf{k}] \omega_{mp} g_{mp}^\omega \left[g_0^\omega \left(\mathcal{G}_{mp}^{ab} - i\frac{\Omega_{mp}^{ab}}{2} \right) \partial_c F_{mp} + g_0^0 \left(\mathcal{G}_{mp}^{ac} - i\frac{\Omega_{mp}^{ac}}{2} \right) \partial_b F_{mp} \right], \quad (25d)$$

$$\chi_{abc}^{\text{HOP}} = -\frac{ie^3}{2\epsilon_0\omega\hbar^2} \sum_{m,p} \int_{\text{BZ}} [d\mathbf{k}] \omega_{mp} g_{mp}^\omega \left[\left(\mathcal{G}_{mp}^{ac} - i\frac{\Omega_{mp}^{ac}}{2} \right) \partial_b g_{mp}^\omega + \left(\mathcal{G}_{mp}^{ab} - i\frac{\Omega_{mp}^{ab}}{2} \right) \partial_c g_{mp}^0 \right] F_{mp}, \quad (25e)$$

$$\chi_{abc}^{\text{DR}} = -\frac{ie^3}{2\epsilon_0\omega\hbar^2} \sum_{m,p} \int_{\text{BZ}} [d\mathbf{k}] \omega_{mp} g_{mp}^\omega \left[g_{mp}^\omega \left(\mathcal{G}_{mp}^{ac} - i\frac{\Omega_{mp}^{ac}}{2} \right) \partial_b F_{mp} + g_{mp}^0 \left(\mathcal{G}_{mp}^{ab} - i\frac{\Omega_{mp}^{ab}}{2} \right) \partial_c F_{mp} \right]. \quad (25f)$$

In the above expressions, $[d\mathbf{k}] = d^d k / (2\pi)^d$ in d spatial dimensions. The NL susceptibilities are primarily determined by four band geometric quantities: the Berry curvature (Ω), the quantum metric (\mathcal{G}), the metric connection (Γ), and the symplectic connection ($\tilde{\Gamma}$) [43, 48–50].

The former two are the real and imaginary parts of the QGT ($\mathcal{Q} = \mathcal{G} - i\Omega/2$), while the latter two are the real and imaginary parts of the QGC ($\mathcal{C} = \Gamma - i\tilde{\Gamma}$), respectively. The functions, $g_{mp}^\omega = [1/\tau - i(\omega - \omega_{mp})]^{-1}$ and $\tilde{g}_{mp}^\omega = [2/\tau - i(\omega - \omega_{mp})]^{-1}$ with $\hbar\omega_{mp} = (\epsilon_{m,\mathbf{k}} - \epsilon_{p,\mathbf{k}})$

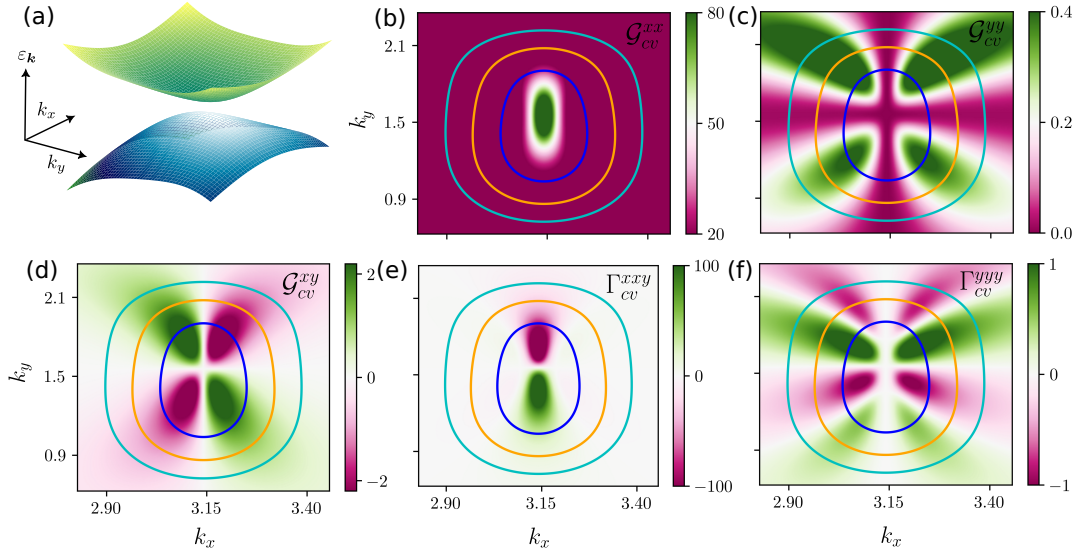


Figure 1. (a) Band dispersion for two dimensional \mathcal{PT} -symmetric CuMnAs. We set the hopping parameters as $t = 0.08$ eV and $\tilde{t} = 1$ eV. The other parameters are $\alpha_R = 0.8$, $\alpha_D = 0$, and $\mathbf{f}_{AF} = (0.85, 0, 0)$ eV. The momentum space distribution of the quantum metric components: (b) \mathcal{G}_{cv}^{xx} , (c) \mathcal{G}_{cv}^{yy} , and (d) \mathcal{G}_{cv}^{xy} . The momentum space distribution of the metric connection (e) Γ_{cv}^{xxy} and (f) Γ_{cv}^{yyy} . We have set the temperature to be $T = 12$ K, and the scattering time $\tau = 10^{-14}$ s for all our calculations.

are related to the joint density of states broadened by disorder. $F_{mp} = f_m^{(0)} - f_p^{(0)}$ is the difference in the occupation of the m and p bands in equilibrium. The Fermi-Dirac distribution function gives the normalized occupation density in the m th band, $f_m^{(0)} = [1 + e^{\beta(\epsilon_{m,\mathbf{k}} - \mu)}]^{-1}$ with $\beta (= 1/k_B T)$. Here, T , μ , and k_B are the thermodynamic temperature, chemical potential, and the Boltzmann constant, respectively.

These NL responses at frequency ω , combined with Eq. (8) complete the theoretical framework of electric field-induced modulation of the RI of a material or the electro-optic effect. The results obtained so far are general and not constrained by any symmetry restrictions. However, different band geometric quantities can either dominate or vanish in systems with specific symmetries, making the induced EO effect an indirect probe of the band geometry of the system. An interesting system is where both \mathcal{P} and \mathcal{T} symmetries are broken, while their combined action, \mathcal{PT} , remains intact [51–54]. In \mathcal{PT} symmetric systems, the Berry curvature and the symplectic connection vanish over the entire Brillouin zone [31]. As a consequence, the electro-optic effect is induced entirely by the quantum metric and the metric connection. The linear order anomalous Hall response also vanishes as the Berry curvature is zero over the entire Brillouin zone in \mathcal{PT} symmetric systems.

In the next section, we apply our theory to a \mathcal{PT} -symmetric model. This will allow us to illustrate the contributions of the quantum metric and the metric connection.

V. Linear Electro-Optic Effect in \mathcal{PT} - symmetric systems

In this section, we study the linear EO effect in CuMnAs, a \mathcal{PT} symmetric antiferromagnet with broken \mathcal{P} and \mathcal{T} symmetry [55–58]. CuMnAs hosts oppositely magnetized sublattices (or Mn atoms - designated as A and B), which break the \mathcal{P} and \mathcal{T} symmetry. However, the simultaneous interchange of the A and B sublattices with a magnetization flip keeps the system unchanged, reflecting its \mathcal{PT} symmetry. The opposite magnetization also leads to sublattice-dependent anti-symmetric spin-orbit coupling. The effective tight-binding Hamiltonian of this system [42, 59] is given by

$$\mathcal{H}(\mathbf{k}) = \begin{pmatrix} \epsilon_0(\mathbf{k}) + \mathbf{f}_A(\mathbf{k}) \cdot \boldsymbol{\sigma} & V_{AB}(\mathbf{k}) \\ V_{AB}(\mathbf{k}) & \epsilon_0(\mathbf{k}) + \mathbf{f}_B(\mathbf{k}) \cdot \boldsymbol{\sigma} \end{pmatrix}. \quad (26)$$

Here, we have $\epsilon_0(\mathbf{k}) = -t(\cos k_x + \cos k_y)$, $V_{AB} = -2\tilde{t} \cos \frac{k_x}{2} \cos \frac{k_y}{2}$, and $\boldsymbol{\sigma}$ represents the Pauli spin matrices. The hopping between orbitals of the same sublattice is quantified by t , while \tilde{t} denotes the hopping between orbitals on different sublattices. The sublattice-dependent spin-orbit coupling and the magnetization field are included in $\mathbf{f}_A(\mathbf{k}) = -\mathbf{f}_B(\mathbf{k})$ and we have,

$$\mathbf{f}_A(\mathbf{k}) = \begin{pmatrix} f_{AF}^x - \alpha_r \sin(k_y) + \alpha_d \sin(k_y) \\ f_{AF}^y + \alpha_r \sin(k_x) + \alpha_d \sin(k_x) \\ f_{AF}^z \end{pmatrix}. \quad (27)$$

The electronic band dispersion of the Hamiltonian in Eq. (26) are given by $\epsilon(\mathbf{k}) = \epsilon_0 \pm \sqrt{V_{ab}^2 + f_{Ax}^2 + f_{Ay}^2 + f_{Az}^2}$, and shown in Fig. 1(a). Here,

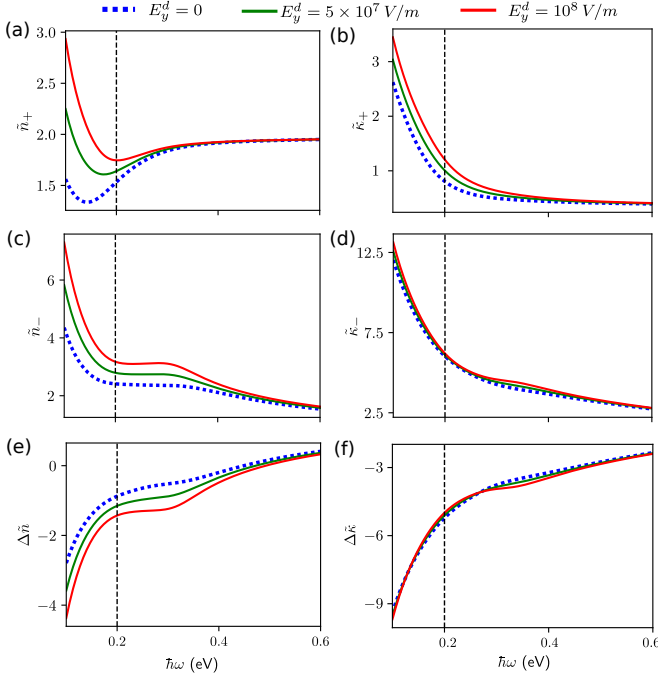


Figure 2. The frequency dependence of the refractivities (a) \tilde{n}_+ and (c) \tilde{n}_- , respectively. (b) and (d) depict the frequency dependence of the absorption coefficients, $\tilde{\kappa}_+$ and $\tilde{\kappa}_-$, respectively. The variation of (e) $\Delta\tilde{n}$ and (f) $\Delta\tilde{\kappa}$ with frequency. The response for different values of the dc electric field, $\mathbf{E}^d = E_y^d \hat{y}$, in (a)-(f) are indicated by the blue dots ($E_y^d = 0$), green line ($E_y^d = 5 \times 10^7$ V/m), and red the line ($E_y^d = 10^8$ V/m) respectively. The dotted vertical line represents $\hbar\omega = \mu$, where μ is the chemical potential. For all our calculations, we have set the temperature to be $T = 12$ K and the scattering time τ to be 10^{-14} s.

$+$ ($-$) denotes the conduction (valence) band. We present the momentum space distribution of different components of the quantum metric and the metric connection in Fig. 1(b)-(f). These components are pivotal for inducing polarization rotation within \mathcal{PT} -symmetric systems. Fig. 3 in Appendix A shows the real and imaginary parts of χ_{xxy} and χ_{yyx} for CuMnAs. As the Berry curvature and symplectic connection vanish for a \mathcal{PT} symmetric system, the shift current is induced by the metric connection, while the other contributions arise from the quantum metric. For CuMnAs, all the contributions of χ_{xxy} and χ_{yyx} components are zero.

In Fig. 2(a) and 2(b), we show the variation of \tilde{n}_+ and $\tilde{\kappa}_+$ with optical frequency. Figure 2(c) and 2(d) show the variation of \tilde{n}_- and $\tilde{\kappa}_-$ with frequency. Since the NL susceptibilities are approximately seven orders smaller than the linear susceptibility, the effect of the dc electric field becomes significant around $E_y^d = 10^7$ V/m or so. Experimentally, external field ($E_y^d = 10^6$ V/m) induced linear EO effect (Pockels effect) has been observed in ferroelectric materials like $\text{C}_8\text{H}_8\text{N}_2$ and LiBNO_3 with birefringence being of the order of $\sim 10^{-5}$ and $\sim 10^{-4}$ respectively [60]. We present the altered bire-

fringence, $\Delta\tilde{n} = \Delta\tilde{n}_+ - \Delta\tilde{n}_-$, as a function of frequency in Fig. 2(e). In Fig. 2(f), we present the dichroism, $\Delta\tilde{\kappa}$, as a function of frequency. We note that in Fig. 3, all the non-monotonic variation of the optical susceptibilities occur for frequencies $\hbar\omega \ll 2\mu$. Beyond the frequencies $\hbar\omega \ll 2\mu$, the nonlinear susceptibilities vanish as $1/\omega$. A similar trend can also be seen in all panels of Fig. 2.

There are two distinct differences between the electro-optic effect in conventional ferroelectric materials and \mathcal{PT} symmetric systems. In contrast to ferroelectric materials, the EO effect in CuMnAs is induced by the band geometric quantities, such as the quantum metric and the metric connection. Additionally, CuMnAs supports the EO effect for optical energies below the chemical potential [see the region to the left of the dashed vertical line for $\mu = 0.2$ eV in Fig. 2]. This is a distinct signature of Fermi surface effects playing a significant role in the total optical susceptibility in metallic systems.

VI. Conclusion

To summarize, our study highlights the intricate phenomena of polarization rotation induced by linear electro-optic effect-induced alteration in their refractive index. Using quantum kinetic theory and density matrix formalism, we have identified six distinct contributions to the linear EO effect: shift, injection, Drude, anomalous, higher-order pole, and double resonant currents. Our work emphasizes the significant roles of the quantum metric and metric connection in \mathcal{PT} -symmetric systems, where Berry curvature and symplectic connection are nullified. We derived expressions for the change in refractive index (RI) and calculated the resulting polarization rotation of emergent light in the presence of a transverse static electric field.

From an application perspective, the electro-optic effect is the cornerstone for electro-optic modulation, which is crucial for precise control of optical parameters. Electro-optic modulators are indispensable optical components for modulating light's intensity (intensity modulators) and phase or polarization (phase modulators) [3–5, 61–63]. In addition to serving as a potential probe for band geometric quantities, efficient EO modulators drive innovation across the diverse fields of optical communications [64, 65], computing [66], microwave [67] and quantum photonics [68–70], sensing [71, 72], and telecommunications [73–75].

VII. Acknowledgement

We acknowledge Debasis Dutta, Kamal Das, and Debottam Mandal for the useful discussions. M.M.K. acknowledges the Department of Science and Technology, Government of India, for financial support via Project No. DST/NM/TUE/QM-6/2019(G)-IIT Kanpur. S. S. thanks the MHRD, India, for funding through the Prime

Minister's Research Fellowship (PMRF).

which leads us to the recursive equation for $\rho^{(N)}$,

$$\rho_{mp}^{(N)} = \frac{e}{\hbar} g_{mp}^{\omega_\Sigma} \mathbf{E} \cdot [\mathcal{D}_\mathbf{k} \rho^{(N-1)}]_{mp} . \quad (\text{A3})$$

A. Optical susceptibility calculations

In this section, we provide a detailed calculation of the optical conductivity using the density matrix up to the second order in the electric field. Perturbatively treating the density matrix in the quantum Liouville equation, the N th order density matrix can be shown to be related to the $(N-1)$ th order density matrix via the recursive relation,

$$\frac{\partial \rho_{mp}^{(N)}}{\partial t} + \frac{i}{\hbar} [\hat{H}_0, \rho^{(N)}]_{mp} + \frac{\rho_{mp}^{(N)}}{\tau/N} = \frac{-ie\mathbf{E}}{\hbar} \cdot [\mathbf{r}, \rho^{(N-1)}]_{mp} . \quad (\text{A1})$$

In the steady state, this simplifies to,

$$\left(-i\omega_\Sigma + i\omega_{mp} + \frac{N}{\tau} \right) \rho_{mp}^{(N)} = \frac{e\mathbf{E}}{\hbar} \cdot [\mathcal{D}_\mathbf{k} \rho^{(N-1)}]_{mp} , \quad (\text{A2})$$

The function $g_{mp}^{\omega_\Sigma} = [N/\tau - i(\omega_\Sigma - \omega_{mp})]^{-1}$ characterizes the density of states broadened by scattering corresponding to incident frequency ω_Σ . Here, ω_Σ and $\omega_{mp} = \hbar^{-1}(\epsilon_{m,\mathbf{k}} - \epsilon_{n,\mathbf{k}})$ are the sum of the harmonic frequencies incident on the system, and difference of the frequencies corresponding to bands indexed m and n , respectively. The first-order density matrix is given by,

$$\rho_{mp}^{(1)} = \frac{e}{\hbar} g_{mp}^{\omega_\Sigma} \mathbf{E} \cdot \left(\partial_\mathbf{k} \rho_{mp}^{(0)} - i[\mathcal{R}_\mathbf{k}, \rho^{(0)}]_{mp} \right) . \quad (\text{A4})$$

Here, $\rho_{mp}^{(0)} = f_m \delta_{mp}$ represents the equilibrium distribution of electrons, with $f_m = [1 + e^{\beta(\epsilon_{m,\mathbf{k}} - \mu)}]^{-1}$ being the Fermi-Dirac distribution for the m th band, and $\beta = 1/(k_B T)$. With some simplifications, the first-order density matrix can be expressed as,

$$\rho_{mp}^{(1)} = \frac{e}{\hbar} g_{mp}^{\omega_\Sigma} (\partial_c f_m + i\mathcal{R}_{mp}^c F_{mp}) E_c e^{-i\omega t} . \quad (\text{A5})$$

We note that for $m = p$, the second term of the above equation vanishes, and for $m \neq p$ the first term vanishes. Calculating the second-order density matrix, we obtain,

$$\rho_{mp}^{(2)} = \frac{e}{\hbar} g_{mp}^{\omega_\Sigma} \mathbf{E} \cdot \left[\partial_\mathbf{k} \rho_{mp}^{(1)} - i[\mathcal{R}_\mathbf{k}, \rho^{(1)}]_{mp} \right] = \frac{e}{\hbar} g_{mp}^{\omega_\Sigma} E_c \left[\partial_c \rho_{mp}^{(1)} - i \sum_n \left(\mathcal{R}_{mn}^c \rho_{np}^{(1)} - \rho_{mn}^{(1)} \mathcal{R}_{np}^c \right) \right] . \quad (\text{A6})$$

For a two-band model, the second-order density matrix can be separated into four parts: two diagonal and two off-diagonal terms. We define them as, $\rho_{mm}^{(2),I}$, $\rho_{mm}^{(2),II}$, $\rho_{mp}^{(2),I}$, and $\rho_{mp}^{(2),II}$, respectively. These four parts after pairwise field symmetrization can be expressed as,

$$\rho_{mm}^{(2),I}(\omega; \omega, 0) = \frac{e^2}{\hbar^2} (\tilde{g}_0^\omega g_0^\omega + \tilde{g}_0^0 g_0^\omega) \partial_c \partial_d f_m E_c E_y^d , \quad (\text{A7})$$

$$\rho_{mm}^{(2),II}(\omega; \omega, 0) = \frac{e^2}{\hbar^2} \tilde{g}_0^\omega \sum_n [(g_{nm}^\omega \mathcal{R}_{mn}^b \mathcal{R}_{nm}^c F_{nm} - g_{mn}^\omega \mathcal{R}_{mn}^c \mathcal{R}_{nm}^b F_{mn}) + (g_{nm}^0 \mathcal{R}_{mn}^c \mathcal{R}_{nm}^b F_{nm} - g_{mn}^0 \mathcal{R}_{mn}^b \mathcal{R}_{nm}^c F_{mn})] , \quad (\text{A8})$$

$$\rho_{mp}^{(2),I}(\omega; \omega, 0) = i \frac{e^2}{\hbar^2} \tilde{g}_{mp}^\omega [(g_{mp}^\omega F_{mp} \mathcal{D}_{mp}^b \mathcal{R}_{mp}^c + \mathcal{R}_{mp}^c \partial_b (g_{mp}^\omega F_{mp})) + (g_{mp}^0 F_{mp} \mathcal{D}_{mp}^c \mathcal{R}_{mp}^b + \mathcal{R}_{mp}^b \partial_c (g_{mp}^0 F_{mp}))] , \quad (\text{A9})$$

$$\rho_{mp}^{(2),II}(\omega; \omega, 0) = i \frac{e^2}{\hbar^2} \tilde{g}_{mp}^\omega [g_0^\omega \mathcal{R}_{mp}^b \partial_c F_{mp} + g_0^0 \mathcal{R}_{mp}^c \partial_b F_{mp}] . \quad (\text{A10})$$

In the above equations, we have considered the frequency combination of $(\omega, 0)$. Further, we calculate the current densities using the definition,

$$\mathbf{j}(t) = -e \text{Tr}[\rho \hat{\mathbf{v}}] . \quad (\text{A11})$$

So, the N th order current can be calculated as,

$$j_a^{(N)}(t) = -e \sum_{m,p} v_{pm}^a \rho_{mp}^{(N)}(t) . \quad (\text{A12})$$

Here, $v_{pm}^a = v_{pm}^{0a} \delta_{pm} + i\omega_{pm} \mathcal{R}_{pm}^a$ is the general velocity operator with $v_{mm}^{0a} = \hbar^{-1} \partial_a \epsilon_m$, and \mathcal{R}_{pm}^q is the q th component

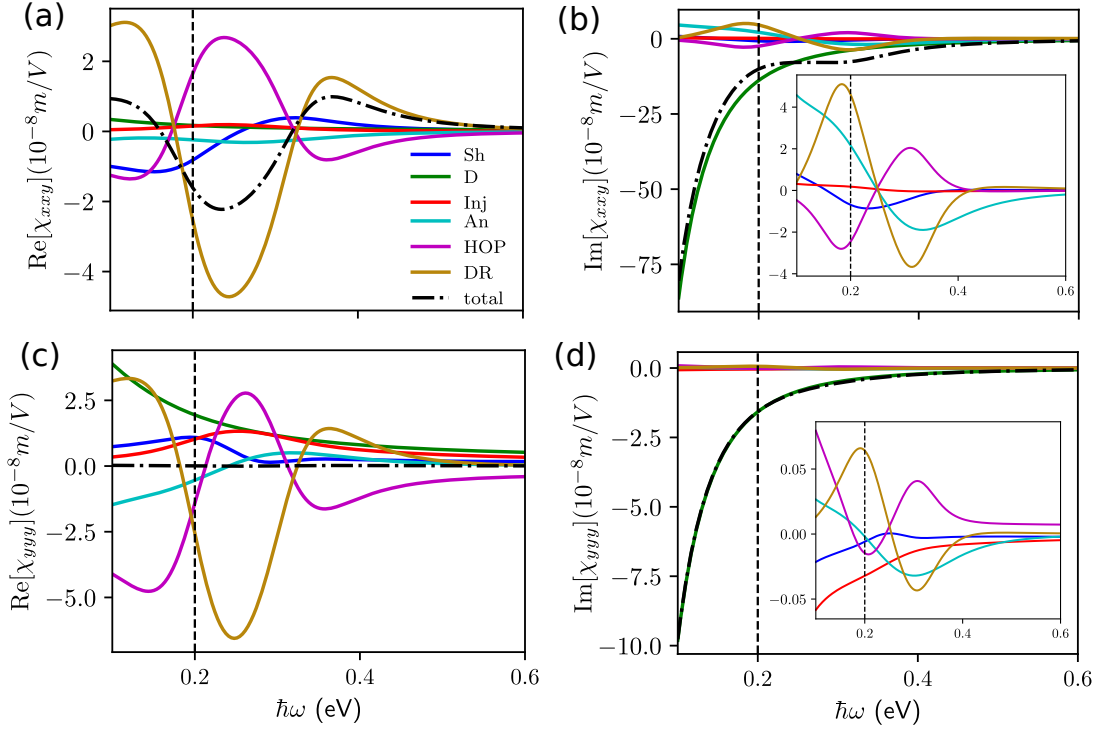


Figure 3. Frequency dependence of various components - shift (Sh), Drude (D), injection (Inj), anomalous (An), higher-order pole (HOP), and double-resonant (DR), of nonlinear susceptibility. Panels (a) and (b) show the real and imaginary parts of the susceptibility χ_{xxy} , respectively. Panels (c) and (d) show the real and imaginary parts of the susceptibility χ_{yyy} , respectively. The susceptibilities without the Drude contribution are shown in the inset of panels (b) and (d). The model parameters are the same as in fig. 1.

of the interband Berry connection. Using Eq. (A12), for $N = 1$, we can write the linear current as,

$$\begin{aligned}
 j_a^{(1)}(t) &= -\frac{e^2}{\hbar} \sum_{m,p} \sum_c g_{mp}^\omega (v_{pm}^{0a} \delta_{pm} + i\omega_{mp} \mathcal{R}_{pm}^a) (\partial_c f_m + i\mathcal{R}_{mp}^c F_{mp}) E^c e^{-i\omega t}, \\
 &= -\frac{e^2}{\hbar} \sum_c \left[\sum_m \frac{1}{\hbar} (\partial_a \epsilon_m) (\partial_c f_m) g_0^\omega - \sum_{m,p} \omega_{mp} g_{mp}^\omega \mathcal{R}_{pm}^a \mathcal{R}_{mp}^c F_{mp} \right] E^c e^{-i\omega t}, \\
 &= -\frac{e^2}{\hbar} \sum_c \left[\sum_m \frac{1}{\hbar} (\partial_a \epsilon_m) (\partial_c f_m) g_0^\omega - \sum_{m,p} \omega_{mp} g_{mp}^\omega \mathcal{Q}_{mp}^{ac} F_{mp} \right] E^c e^{-i\omega t}. \quad (\text{A13})
 \end{aligned}$$

The product of two Berry connections has been expressed in terms of the QGT. It can be expressed in terms of the band-resolved Berry curvature and the quantum metric as,

$$\mathcal{Q}_{mp}^{bc} = \mathcal{R}_{pm}^b \mathcal{R}_{mp}^c = \mathcal{G}_{mp}^{bc} - (i/2) \Omega_{mp}^{bc}. \quad (\text{A14})$$

We have two contributions to the current density. Under \mathcal{PT} symmetry, as the Berry curvature vanishes, the linear conductivity corresponding to each of the contributions

can therefore be given as,

$$\sigma_{ac}^{\text{intra}}(\omega) = -\frac{e^2}{\hbar} \sum_m \int [d\mathbf{k}] \frac{1}{\hbar} (\partial_a \epsilon_m) g_0^\omega (\partial_c f_m^{(0)}), \quad (\text{A15})$$

$$\sigma_{ac}^{\text{inter}}(\omega) = \frac{e^2}{\hbar} \sum_{m,p} \int [d\mathbf{k}] \omega_{mp} g_{mp}^\omega \mathcal{G}_{mp}^{ac} F_{mp}. \quad (\text{A16})$$

The linear conductivity $\sigma_{ac}(\omega)$ is given as,

$$\sigma_{ac}(\omega) = \sigma_{ac}^{\text{intra}}(\omega) + \sigma_{ac}^{\text{inter}}(\omega). \quad (\text{A17})$$

The corresponding susceptibility tensor is given from $\sigma_{ac}(\omega) = -i\omega\epsilon_0\chi_{ac}(\omega)$, where ϵ_0 is the permittivity of vacuum. It can be shown that the intraband conductivity

ity is the infamous Drude conductivity [34] for frequency-dependent electric fields and that the interband contribution we see for $\sigma_{ac}^{\text{inter}}(\omega)$, is the linear anomalous Hall conductivity [76]. As the Berry curvature vanishes in a \mathcal{PT} -symmetric system, the total linear contribution to the

interband conductivity would be from the quantum metric. At $N = 2$ in Eq. (A12), we get the second-order current. The expressions of the pairwise field-symmetrized second-order susceptibilities are shown in the main text.

-
- [1] Chun-Ching Shih and A Yariv, “A theoretical model of the linear electro-optic effect,” *Journal of Physics C: Solid State Physics* **15**, 825 (1982).
 - [2] R.W. Boyd, *Nonlinear Optics*, Electronics & Electrical (Academic Press, 2003).
 - [3] Li Chen, Qiang Xu, Michael G. Wood, and Ronald M. Reano, “Hybrid silicon and lithium niobate electro-optical ring modulator,” *Optica* **1**, 112–118 (2014).
 - [4] Mingxiao Li, Jingwei Ling, Yang He, Usman A. Javid, Shixin Xue, and Qiang Lin, “Lithium niobate photonic-crystal electro-optic modulator,” *Nature Communications* **11**, 4123 (2020).
 - [5] Cheng Wang, Mian Zhang, Xi Chen, Maxime Bertrand, Amirhassan Shams-Ansari, Sethumadhavan Chandrasekhar, Peter Winzer, and Marko Lončar, “Integrated lithium niobate electro-optic modulators operating at cmos-compatible voltages,” *Nature* **562**, 101–104 (2018).
 - [6] Robert Goldstein, “Electro-optic devices in review,” *Lasers Appl* **5**, 67–73 (1986).
 - [7] Ernesta M Meintjes and R E Raab, “A new theory of pockels birefringence in non-magnetic crystals,” *Journal of Optics A: Pure and Applied Optics* **1**, 146 (1999).
 - [8] Zijian Cui, Dean Liu, Jie Miao, Aihua Yang, and Jianqiang Zhu, “Phase matching using the linear electro-optic effect,” *Phys. Rev. Lett.* **118**, 043901 (2017).
 - [9] Christopher J. Gibson, Patrick Bevington, Gian-Luca Oppo, and Alison M. Yao, “Control of polarization rotation in nonlinear propagation of fully structured light,” *Phys. Rev. A* **97**, 033832 (2018).
 - [10] Y. Liu, M.T. Hill, E. Tangdiongga, H. de Waardt, N. Calabretta, G.D. Khoe, and H.J.S. Dorren, “Wavelength conversion using nonlinear polarization rotation in a single semiconductor optical amplifier,” *IEEE Photonics Technology Letters* **15**, 90–92 (2003).
 - [11] Dajin Luo, Huajie Hu, Churong Pan, Yingxin Zhang, Yan Qin, Haixia Chen, Dong Wei, Hong Gao, and Fuli Li, “Nonlinear control of polarization rotation of hybrid-order vector vortex beams,” *Journal of Optics* **22**, 115612 (2020).
 - [12] Guanyu Ye, Kin Kee Chow, Bowen Liu, Maolin Dai, Yifan Ma, Takuma Shirahata, Shinji Yamashita, and Sze Yun Set, “L-band mode-locked fiber laser using all polarization-maintaining nonlinear polarization rotation,” *Opt. Lett.* **48**, 4729–4732 (2023).
 - [13] Ileana-Cristina Benea-Chelms, Maryna L. Meretska, Delwin L. Elder, Michele Tamagnone, Larry R. Dalton, and Federico Capasso, “Electro-optic spatial light modulator from an engineered organic layer,” *Nature Communications* **12**, 5928 (2021).
 - [14] Meng-Jia Sun, Chao Zheng, Yuan Gao, Andrew Johnston, Amin Morteza Najarian, Pei-Xi Wang, Oleksandr Voznyy, Sjoerd Hoogland, and Edward H. Sargent, “Linear electro-optic modulation in highly polarizable organic perovskites,” *Advanced Materials* **33**, 2006368 (2021).
 - [15] L M Blinov, “Electro-optical effects in liquid crystals,” *Soviet Physics Uspekhi* **17**, 658–672 (1975).
 - [16] Jing Ma and D. A. Pesin, “Chiral magnetic effect and natural optical activity in metals with or without weyl points,” *Phys. Rev. B* **92**, 235205 (2015).
 - [17] Kabyashree Sonowal, Ashutosh Singh, and Amit Agarwal, “Giant optical activity and kerr effect in type-i and type-ii weyl semimetals,” *Phys. Rev. B* **100**, 085436 (2019).
 - [18] Ashutosh Singh, Saikat Ghosh, and Amit Agarwal, “Nonlinear and anisotropic polarization rotation in two-dimensional dirac materials,” *Phys. Rev. B* **97**, 205420 (2018).
 - [19] Susumu Namba, “Electro-optical effect of zincblende,” *JOSA* **51**, 76–79 (1961).
 - [20] Meijuan Cheng, Shunqing Wu, Zi-Zhong Zhu, and Guang-Yu Guo, “Large second-harmonic generation and linear electro-optic effect in trigonal selenium and tellurium,” *Phys. Rev. B* **100**, 035202 (2019).
 - [21] Huaxiang Fu and Ronald E. Cohen, “Polarization rotation mechanism for ultrahigh electromechanical response in single-crystal piezoelectrics,” *Nature* **403**, 281–283 (2000).
 - [22] Zhijun Jiang, Charles Paillard, Hongjun Xiang, and L. Bellaiche, “Linear versus nonlinear electro-optic effects in materials,” *Phys. Rev. Lett.* **125**, 017401 (2020).
 - [23] Koen Alexander, John P. George, Jochem Verbist, Kristiaan Neyts, Bart Kuyken, Dries Van Thourhout, and Jeroen Beeckman, “Nanophotonic pockels modulators on a silicon nitride platform,” *Nature Communications* **9**, 3444 (2018).
 - [24] Mathias Berciano, Guillaume Marcaud, Pedro Damas, Xavier Le Roux, Paul Crozat, Carlos Alonso Ramos, Diego Pérez Galacho, Daniel Benedikovic, Delphine Marris-Morini, Eric Cassan, and Laurent Vivien, “Fast linear electro-optic effect in a centrosymmetric semiconductor,” *Communications Physics* **1**, 64 (2018).
 - [25] T. Fujiwara, “Comparison of electro-optic effect between stoichiometric and congruent linbo₃,” *Electronics Letters* **35**, 499–501(2) (1999).
 - [26] GE Peterson, AA Ballman, PV Lenzo, and PM Bridenbaugh, “Electro-optic properties of linbo₃,” *Applied Physics Letters* **5**, 62–64 (1964).
 - [27] I. P. Kaminow and W. D. Johnston, “Quantitative determination of sources of the electro-optic effect in linbo₃ and litao₃,” *Phys. Rev.* **160**, 519–522 (1967).
 - [28] Yufeng Wang, Laxmi Adhikari, Gary A. Baker, and G. J. Blanchard, “Cation structure-dependence of the pockels effect in aprotic ionic liquids,” *Phys. Chem. Chem. Phys.* **24**, 18067–18072 (2022).
 - [29] Mo Li and Hong X. Tang, “Strong pockels materials,” *Nature Materials* **18**, 9–11 (2019).
 - [30] Zhi Li, Yuewen Gao, Yu Gu, Shengli Zhang, Toshiaki

- Iitaka, and W. M. Liu, “Berry curvature induced linear electro-optic effect in chiral topological semimetals,” *Phys. Rev. B* **105**, 125201 (2022).
- [31] Pankaj Bhalla, Kamal Das, Dimitrie Culcer, and Amit Agarwal, “Resonant second-harmonic generation as a probe of quantum geometry,” *Phys. Rev. Lett.* **129**, 227401 (2022).
- [32] D.J. Griffiths, *Introduction to Electrodynamics*, v. 2 (Cambridge University Press, 2017).
- [33] J.D. Jackson, *Classical Electrodynamics* (Wiley, 2012).
- [34] N.W. Ashcroft, N.D. Mermin, and N.D. Mermin, *Solid State Physics*, HRW international editions (Holt, Rinehart and Winston, 1976).
- [35] M.L. Cohen and S.G. Louie, *Fundamentals of Condensed Matter Physics* (Cambridge University Press, 2016).
- [36] S. Visnovsky, *Optics in Magnetic Multilayers and Nanostructures* (Optical Science and Engineering (CRC Press, 2018).
- [37] Xiaoyan Cui, Alexander G. Shtukenberg, John Freudenthal, Shane Nichols, and Bart Kahr, “Circular birefringence of banded spherulites,” *Journal of the American Chemical Society* **136**, 5481–5490 (2014).
- [38] L.D. Landau, J.S. Bell, M.J. Kearsley, L.P. Pitaevskii, E.M. Lifshitz, and J.B. Sykes, *Electrodynamics of Continuous Media, COURSE OF THEORETICAL PHYSICS* (Elsevier Science, 2013).
- [39] J. E. Sipe and A. I. Shkrebtii, “Second-order optical response in semiconductors,” *Phys. Rev. B* **61**, 5337–5352 (2000).
- [40] Claudio Aversa and J. E. Sipe, “Nonlinear optical susceptibilities of semiconductors: Results with a length-gauge analysis,” *Phys. Rev. B* **52**, 14636–14645 (1995).
- [41] Alireza Taghizadeh, F. Hipolito, and T. G. Pedersen, “Linear and nonlinear optical response of crystals using length and velocity gauges: Effect of basis truncation,” *Phys. Rev. B* **96**, 195413 (2017).
- [42] Kamal Das, Shibalik Lahiri, Rhonald Burgos Atencia, Dimitrie Culcer, and Amit Agarwal, “Intrinsic nonlinear conductivities induced by the quantum metric,” *Phys. Rev. B* **108**, L201405 (2023).
- [43] Debottam Mandal, Sanjay Sarkar, Kamal Das, and Amit Agarwal, “Quantum geometry induced third order nonlinear transport responses,” (2024), [arXiv:2310.19092 \[cond-mat.mes-hall\]](https://arxiv.org/abs/2310.19092).
- [44] Harsh Varshney, Kamal Das, Pankaj Bhalla, and Amit Agarwal, “Quantum kinetic theory of nonlinear thermal current,” *Phys. Rev. B* **107**, 235419 (2023).
- [45] Junyeong Ahn, Guang-Yu Guo, and Naoto Nagaosa, “Low-frequency divergence and quantum geometry of the bulk photovoltaic effect in topological semimetals,” *Phys. Rev. X* **10**, 041041 (2020).
- [46] Shengru Han, Liangting Ye, Yang Li, and Bing Huang, “Theoretical understanding of nonlinear optical properties in solids: A perspective,” *The Journal of Physical Chemistry Letters* **15**, 3323–3335 (2024), pMID: 38498006.
- [47] Pankaj Bhalla, Kamal Das, Amit Agarwal, and Dimitrie Culcer, “Quantum kinetic theory of nonlinear optical currents: Finite fermi surface and fermi sea contributions,” *Phys. Rev. B* **107**, 165131 (2023).
- [48] Di Xiao, Ming-Che Chang, and Qian Niu, “Berry phase effects on electronic properties,” *Rev. Mod. Phys.* **82**, 1959–2007 (2010).
- [49] Vladyslav Kozii, Alexander Avdoshkin, Shudan Zhong, and Joel E. Moore, “Intrinsic anomalous hall conductivity in a nonuniform electric field,” *Phys. Rev. Lett.* **126**, 156602 (2021).
- [50] RADU PURICE, *Journal of Operator Theory* **35**, 373–376 (1996).
- [51] Shiqi Xia, Dimitrios Kaltsas, Daohong Song, Ioannis Komis, Jingjun Xu, Alexander Szameit, Hrvoje Buljan, Konstantinos G. Makris, and Zhigang Chen, “Nonlinear tuning of pt symmetry and non-hermitian topological states,” *Science* **372**, 72–76 (2021).
- [52] F. Klauck, L. Teuber, M. Ornigotti, M. Heinrich, S. Scheel, and A. Szameit, “Observation of pt-symmetric quantum interference,” *Nature Photonics* **13**, 883–887 (2019).
- [53] Mark Kremer, Tobias Biesenthal, Lukas J. Maczewsky, Matthias Heinrich, Ronny Thomale, and Alexander Szameit, “Demonstration of a two-dimensional pt-symmetric crystal,” *Nature Communications* **10**, 435 (2019).
- [54] Apoorv Tiwari and Tomáš Bzdušek, “Non-abelian topology of nodal-line rings in \mathcal{PT} -symmetric systems,” *Phys. Rev. B* **101**, 195130 (2020).
- [55] Peizhe Tang, Quan Zhou, Gang Xu, and Shou-Cheng Zhang, “Dirac fermions in an antiferromagnetic semimetal,” *Nature Physics* **12**, 1100–1104 (2016).
- [56] Jin Cao, Wei Jiang, Xiao-Ping Li, Daifeng Tu, Jiadong Zhou, Jianhui Zhou, and Yugui Yao, “In-plane anomalous hall effect in \mathcal{PT} -symmetric antiferromagnetic materials,” *Phys. Rev. Lett.* **130**, 166702 (2023).
- [57] W. B. Rui, Moritz M. Hirschmann, and Andreas P. Schnyder, “ \mathcal{PT} -symmetric non-hermitian dirac semimetals,” *Phys. Rev. B* **100**, 245116 (2019).
- [58] P. Wadley, B. Howells, J. Železný, C. Andrews, V. Hills, R. P. Campion, V. Novák, K. Olejník, F. Maccheronzi, S. S. Dhesi, S. Y. Martin, T. Wagner, J. Wunderlich, F. Freimuth, Y. Mokrousov, J. Kuneš, J. S. Chauhan, M. J. Grzybowski, A. W. Rushforth, K. W. Edmonds, B. L. Gallagher, and T. Jungwirth, “Electrical switching of an antiferromagnet,” *Science* **351**, 587–590 (2016).
- [59] Hikaru Watanabe and Youichi Yanase, “Chiral photocurrent in parity-violating magnet and enhanced response in topological antiferromagnet,” *Phys. Rev. X* **11**, 011001 (2021).
- [60] Yohei Uemura, Satoshi Matsuoka, Jun’ya Tsutsumi, Sachio Horiuchi, Shunto Arai, and Tatsuo Hasegawa, “Birefringent field-modulation imaging of transparent ferroelectrics,” *Phys. Rev. Appl.* **14**, 024060 (2020).
- [61] Jeffrey D. Bull, Nicolas A.F. Jaeger, Hiroshi Kato, Mark Fairburn, Adam Reid, and Pejman Ghanipour, “40-GHz electro-optic polarization modulator for fiber optic communications systems,” in *Photonics North 2004: Optical Components and Devices*, Vol. 5577, edited by John C. Armitage, Simon Fafard, Roger A. Lessard, and George A. Lampropoulos, International Society for Optics and Photonics (SPIE, 2004) pp. 133 – 143.
- [62] Ali Forouzmand and Hossein Mosallaei, “Electro-optical amplitude and phase modulators based on tunable guided-mode resonance effect,” *ACS Photonics* **6**, 2860–2869 (2019).
- [63] Mian Zhang, Brandon Buscaino, Cheng Wang, Amirhasan Shams-Ansari, Christian Reimer, Rongrong Zhu, Joseph M. Kahn, and Marko Lončar, “Broadband electro-optic frequency comb generation in a lithium niobate microring resonator,” *Nature* **568**, 373–377 (2019).

- [64] E.L. Wooten, K.M. Kissa, A. Yi-Yan, E.J. Murphy, D.A. Lafaw, P.F. Hallemeier, D. Maack, D.V. Attanasio, D.J. Fritz, G.J. McBrien, and D.E. Bossi, “A review of lithium niobate modulators for fiber-optic communications systems,” *IEEE Journal of Selected Topics in Quantum Electronics* **6**, 69–82 (2000).
- [65] Ileana-Cristina Benea-Chelms, Sydney Mason, Maryna L. Meretska, Delwin L. Elder, Dmitry Kazakov, Amirhassan Shams-Ansari, Larry R. Dalton, and Federico Capasso, “Gigahertz free-space electro-optic modulators based on mie resonances,” *Nature Communications* **13**, 3170 (2022).
- [66] Kevin Portner, Manuel Schmuck, Paul Lehmann, Christoph Weilenmann, Christian Haffner, Ping Ma, Juerg Leuthold, Mathieu Luisier, and Alexandros Emboras, “Analog nanoscale electro-optical synapses for neuromorphic computing applications,” *ACS Nano* **15**, 14776–14785 (2021), pMID: 34459580.
- [67] David Marpaung, Jianping Yao, and José Capmany, “Integrated microwave photonics,” *Nature Photonics* **13**, 80–90 (2019).
- [68] Chen Sun, Mark T. Wade, Yunsup Lee, Jason S. Orcutt, Luca Alloatti, Michael S. Georgas, Andrew S. Waterman, Jeffrey M. Shainline, Rimas R. Avizienis, Sen Lin, Benjamin R. Moss, Rajesh Kumar, Fabio Pavanello, Amir H. Atabaki, Henry M. Cook, Albert J. Ou, Jonathan C. Leu, Yu-Hsin Chen, Krste Asanović, Rajeev J. Ram, Miloš A. Popović, and Vladimir M. Stojanović, “Single-chip microprocessor that communicates directly using light,” *Nature* **528**, 534–538 (2015).
- [69] David R. Carlson, Daniel D. Hickstein, Wei Zhang, Andrew J. Metcalf, Franklyn Quinlan, Scott A. Diddams, and Scott B. Papp, “Ultrafast electro-optic light with subcycle control,” *Science* **361**, 1358–1363 (2018).
- [70] Michał Karpiński, Michał Jachura, Laura J. Wright, and Brian J. Smith, “Bandwidth manipulation of quantum light by an electro-optic time lens,” *Nature Photonics* **11**, 53–57 (2017).
- [71] Ileana-Cristina Benea-Chelms, Sydney Mason, Maryna L. Meretska, Delwin L. Elder, Dmitry Kazakov, Amirhassan Shams-Ansari, Larry R. Dalton, and Federico Capasso, “Gigahertz free-space electro-optic modulators based on mie resonances,” *Nature Communications* **13**, 3170 (2022).
- [72] Dilip K. Prasad, Deepu Rajan, Lily Rachmawati, Eshan Rajabally, and Chai Quek, “Video processing from electro-optical sensors for object detection and tracking in a maritime environment: A survey,” *IEEE Transactions on Intelligent Transportation Systems* **18**, 1993–2016 (2017).
- [73] Larry Dalton, “Organic electro-optic materials,” in *Conjugated Polymers* (CRC Press, 2019) pp. 299–327.
- [74] Santosh Kumar, Sanjeev Kumar Raghuvanshi, and B. M. A. Rahman, “Design of universal shift register based on electro-optic effect of linbo3 in mach–zehnder interferometer for high speed communication,” *Optical and Quantum Electronics* **47**, 3509–3524 (2015).
- [75] A. V. Krasavin and A. V. Zayats, “Photonic signal processing on electronic scales: Electro-optical field-effect nanoplasmonic modulator,” *Phys. Rev. Lett.* **109**, 053901 (2012).
- [76] Naoto Nagaosa, Jairo Sinova, Shigeki Onoda, A. H. MacDonald, and N. P. Ong, “Anomalous hall effect,” *Rev. Mod. Phys.* **82**, 1539–1592 (2010).